

# Optimization-Based Study of Bend-Twist Coupled Rotor Blades for Passive and Integrated Passive/Active Load Alleviation

*C.L. Bottasso\*, F. Campagnolo, A. Croce, C. Tibaldi*

Dipartimento di Ingegneria Aerospaziale, Politecnico di Milano, Milano, Italy

Scientific Report DIA-SR 11-02,  
5 December 2011

## Abstract

This work is concerned with the design of wind turbine blades with bend-twist coupling, which is obtained here by exploiting the orthotropic properties of composite materials by rotating the fibers away from the pith axis. A set of different blades is designed with a multi-level constrained optimization procedure, based on combined cross sectional, multibody aero-servo-elastic and three dimensional finite element models. The design optimizer sizes all structural elements such that the blade has the lowest possible weight while satisfying a set of design constraints, which include, among others, maximum and fatigue loads, maximum tip deflection and placement of natural frequencies. All designed blades, having the same performance in terms of annual energy production and satisfying exactly the same design requirements, are compared in terms of blade mass, load mitigation and actuator duty cycle.

The first part of this study investigates the possible configurations for achieving bend-twist coupling. At first, fully coupled blades are designed by rotating the fibers for the whole blade span, and a best compromise solution is found to limit weight increase by rotations both in the spar caps and in the skin of the blade. Next, partially coupled blades are designed where fibers are rotated only on the outboard part of the blade, this way achieving good load mitigation capabilities together with weight savings.

Finally, the best configuration of the passive coupled blade is combined with an active individual pitch controller. The synergistic use of passive and active load mitigation technologies is shown to allow for significant load reductions, while at the same time limiting the increase in actuator duty cycle thanks to the opposite effects on this performance metric of the passive and active control solutions.

---

\*Corresponding author, Dipartimento di Ingegneria Aerospaziale, Politecnico di Milano, Milano, Via La Masa 34, 20156 Italy. E-mail: [carlo.bottasso@polimi.it](mailto:carlo.bottasso@polimi.it); Tel.: +39-02-2399-8315; Fax: +39-02-2399-8334.

## Notation

ADC	Actuator duty cycle
AEP	Annual energy production
BTC	Bend-twist coupling
CAD	Computer aided design
DEL	Damage equivalent load
DLC	Design load case
EOG	Extreme operative gust
FEM	Finite element method
HAWT	Horizontal axis wind turbine
IPC	Individual pitch control
LQR	Linear quadratic regulator
MW	Mega Watt
PID	Proportional integral derivative
RPM	Revolutions per minute
SQP	Sequential quadratic programming

## 1 Introduction

Load reduction techniques for wind turbines can be broadly categorized into two families: active and passive. The former aims at reducing loads by actively controlling the machine (for example by changing the blade pitch and the generator torque, or by moving flaps and/or tabs or other active devices), while the latter is based on the idea of designing a structure that, when loaded, deforms so as to induce a load reduction. The classical solution to achieve this structural behavior has been to design blades with some degree of bend-twist coupling (BTC). In fact BTC implies that, when the blade bends because of increased loads, the ensuing change of twist will affect the aerodynamic loading through a change in angle of attack. Passive load mitigation by BTC can be obtained by exploiting the anisotropic mechanical properties of composite materials [1, 2], as done in the present work, and/or by sweeping the blade [3, 4].

This form of load alleviation is in principle very attractive because of its passive nature: there are no actuators which may fail, no moving parts which may wear out, and no need for sensors, all characteristics that are very interesting for wind turbines where simplicity, low maintenance and high availability are key to reducing the cost of energy.

However, as usual in the design of wind turbines or other complex engineering systems, the benefits of BTC blades may be accompanied by other undesirable effects, such as an increase of weight, and of manufacturing complexity and possibly cost. For example, when BTC is obtained by moving the fiber directions away from the blade axis, one also obtains a reduction of the bending stiffness as a side effect. For blades where the bending stiffness is dictated by the satisfaction of the maximum blade tip deflection and/or the placement of the first flap frequency, one then needs to restore it by, for example, increasing the thickness of the spar caps, which will in turn imply some weight increase.

Passive load mitigation by BTC for Horizontal Axis Wind Turbines (HAWTs) has been studied extensively in the literature.

Initially, BTC was introduced to twist the blade so as to increase the angle of attack, thereby anticipating stall and cutting peak loads in stall-controlled rotors [5]. This approach showed a potential for augmenting power capacity, because lowering peak loads allowed for increased rotor

diameters, but it also induced substantial increase in fatigue damage and made the blade prone to flutter [6].

A second, opposite, approach was to twist the blade sections so as to decrease the angle of attack [6, 7], the so called twist-to-feather concept. This method showed significant fatigue damage reduction. To analyze the behavior of such design solution, aeroelastic simulation models were developed where the level of coupling between blade bending and twisting was obtained by directly modifying the beam stiffness sectional properties.

Ong and Tsai [8] showed a way to obtain the desired coupling effects by rotating the composite material fibers away from the blade pitch axis in a D-spar configuration. In their work, the coupling and its limits were investigated both analytically and experimentally. Griffin [9] performed a parametric analysis to understand the tradeoffs between material cost and achievable coupling, studying different material types and different fiber angles. His conclusions indicate an increase in cost for all considered solutions. Among others, de Goeij and his coauthors [10] studied different blade structural configurations to better achieve coupling. They concluded that single or double box design solutions are preferable because they reduce fatigue damage in the connection areas.

References [11, 12, 13, 14, 15] describe the design and testing of a 9-meter stall-controlled blade with 20 deg off-pitch axis unidirectional carbon fibers in the skin from the 25% span location outwards. Results of these efforts showed a reduction in fatigue damage with respect of a baseline model without BTC coupling, but also designed for a different maximum tip deflection. Studies on small blades of similar size are also reported in Refs. [16, 17, 18].

Recently, Capellaro and Kühn [19] have investigated BTC obtained by rotating the plies of the spar caps by 5 and 10 deg, while at the same time increasing the spar cap thickness to keep the same maximum tip displacement. In their models, they used carbon fibers in the spar caps because of the better coupling performance that was obtained when compared to the use of fiber glass. Their results report reductions in damage equivalent loads (DEL) as well as maximum loads.

The literature clearly shows the potential benefits of BTC. Many parametric studies have been performed using models of different levels of complexity and fidelity, yielding a good insight on what can be expected by the adoption of such a technological solution. However, to the authors' knowledge, a comprehensive approach to the design of such complex structures is still lacking. In fact, when designing for a specific set of given conditions (e.g., rated power, wind class, rotor diameter, max tip deflection, etc.), one should be able to compare alternative solutions that all satisfy the same design constraints. Only if all alternatives are fully viable, one can then identify the one that is the most desirable according to given criteria or performance metrics.

This aspect is of crucial importance in the design of blades for large modern wind turbines, given the complex couplings that exist among the various design requirements. For example, as mentioned before, changes in bending stiffness due to fiber rotation must be compensated by increasing the thickness of spars and skin, or by using more performing materials, so as to satisfy max deflections and frequency placement constraints. However, these changes will not only influence weight, but also fatigue and buckling. In turn, the satisfaction of the fatigue and buckling constraints will again influence the sizing of the various structural members of the blade, creating a further coupling. Many other subtle effects are present: for example, different degrees of BTC will induce different mean deflected blade configurations at each mean wind speed, thereby affecting trim and hence power. To restore power to the same level, again so as to perform meaningful comparisons among different candidate solutions with different degrees of BTC, one should then change the trim pitch setting, and this will in turn modify loads, which will again induce a coupling effect in the design.

Unless all these couplings are duly taken into account, the understanding of the real benefits of BTC remain obscure. Unfortunately, approaching the problem by parametric studies is a daunting task, which requires many iterations so as to arrive to the simultaneous satisfaction of all design constraints and the identification of fully viable alternative designs.

A contribution of the present work is to show how a multi-disciplinary optimization approach to blade design can be used for studying the effects of BTC. In this work, blade design is performed with a constrained optimization-based procedure that sizes the structural blade elements by minimizing a cost function [20]. All design requirements are treated as constraints, therefore all converged solutions are viable according to the conditions that have been imposed by the designer, and therefore they could all be adopted. The design optimization software, an evolution described in Ref. [21] of the one developed in Ref. [20], performs the design using a multi-level approach. The method includes 2D finite element models for sectional characterization and analysis, aero-servo-elastic multibody models for load calculation according to certification rules [22, 23], and detailed 3D finite element models for detailed stress-strain, fatigue and buckling analysis. The optimizer operates at and iterates among the various levels, so as to deliver in reasonable computational times a cost-minimizing design solution that also satisfies all desired design constraints at the finest description level, i.e. the detailed 3D model.

Using these automated design tools, in the present work we investigate the effects of BTC, twisting towards feather, identifying the optimal fiber rotation configuration for a 2MW wind turbine blade. Furthermore, we consider blades with partial BTC, i.e. where fibers are rotated only on the outboard portion of the blade span. This seems to lower fatigue damage towards the blade max chord sections while at the same time avoiding reductions in the bending stiffness in the inboard part of the blade, two effects that help in reducing the overall blade weight.

One of the results of this investigation is to show that, by properly designing a partially coupled BTC blade, one not only can achieve significant load alleviation with a lighter blade, but also the pitch actuator duty cycle (ADC) is much reduced. In fact, since the blade self-reacts to turbulent fluctuations in the wind, the control system has to pitch the blades less in response to wind disturbances.

This result is of potential interest, because it opens the way to a synergistic combination of passive and active load control technologies, which is also explored in this paper. In fact, individual pitch control (IPC), an active control technique where each blade is independently actuated to reduce the effects of deterministic and non-deterministic disturbances [24], has been shown to reduce loads at the expense of an increase in pitch activity [25, 26, 27, 28, 29, 30, 31, 32, 33, 24]. This often much increased ADC requires suitably designed pitch systems that can withstand the wear induced by IPC, and this has an effect on cost, complexity and maintenance.

However, since BTC and IPC can both mitigate loads, but BTC reduces ADC while IPC increases it, there is a potential synergistic effect of the two technologies. Therefore, it appears possible to have a combined load reduction effect, larger than one would get by adopting one single technology, while limiting the effects on ADC.

To explore these ideas and discuss the design of BTC blades and the combination of BTC and IPC technology, the paper has been organized according to the following plan. At first, we describe the optimization-based multi-level method for blade design in Section 2. Next, we present the results of a parametric study on the design of coupled blades in Section 3, starting from a 2MW uncoupled blade which is taken as baseline for all comparisons. In § 3.1 we study the fully coupled case, and identify a configuration of best compromise, where fibers are rotated throughout the whole span of the blade both in the skin and the spar caps; such a solution is shown to limit the effects of weight increase due to the rotation of the fibers and the subsequent need to restore stiffness for the satisfaction of the design constraints. In § 3.2 we consider the case

of partial coupling, limiting fiber rotations only on an outboard section of the blade span. We identify a configuration that retains good load mitigation ability, but that is also of reduced weight when compared to the baseline uncoupled blade. Finally, in Section 4 we study the combination of the passive partially coupled blade with an active IPC controller. By tuning the controller in a more or less aggressive way, we show the possible tradeoffs that can be achieved between load mitigation and ADC increase. The paper is concluded in Section 5, where we discuss the main findings of the present investigation.

## 2 Optimization-based Multi-level Method for Blade Design

Optimization tools for rotor blades have been recently developed to aid the design process of these complex structures, and a review of the literature is offered in Ref. [20]. In this work, we use the design approach developed in Ref. [21] based on the earlier results of Ref. [20], and implemented in the code *Cp-Max* (*C*ode for *P*erformance *M*aximization). For computational efficiency, the design is performed as a sequence of nested optimizations that operate at various description levels of the blade: a quasi-3D “coarse” representation which is made up of a 2D FEM cross-sectional model together with a spatial beam model, and a detailed “fine” 3D FEM model.

Using *Cp-Max*, a structural blade optimization problem for given aerodynamic shape, which is the case considered here, is conducted as described in the following and shown in Figure 1.

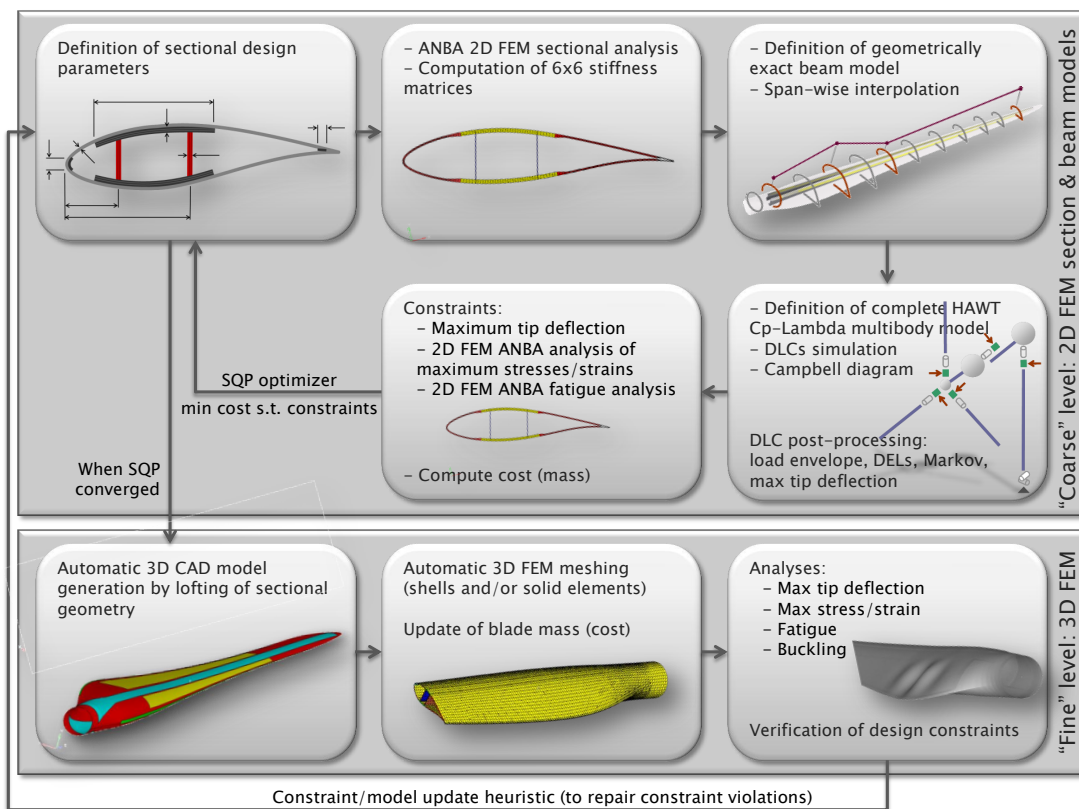


Fig. 1: Multi-level structural blade optimization problem for given aerodynamic shape.

At first, the blade structural configuration and material properties are defined. Next, the sectional structural configuration is parameterized, thereby defining the design variables, which

include the thickness of skin, shear webs, spar caps, and the area of leading and trailing edge reinforcements. Such variables are defined for selected span-wise stations, and interpolated elsewhere along the span using shape functions.

Sectional models are defined using either 2D finite element meshes modeling the stack sequence of plies or using equivalent panels. From the sectional models, fully-populated stiffness matrices are computed using the code ANBA (Anisotropic Beam Analysis), based on the anisotropic beam theory of Ref. [34]. The stiffness matrices obtained in this way are used for defining a geometrically exact shear and torsion-deformable beam model [35].

The resulting beam is used in a complete aero-servo-elastic model of the machine, implemented here with the comprehensive non-linear finite-element-based multibody dynamics simulator Cp-Lambda (Code for Performance, Loads, Aero-Elasticity by Multi-Body Dynamic Analysis) [36, 37].

The model is completed by a regulation strategy [38] and a collective-pitch/torque controller, based here on a speed-scheduled linear quadratic regulator (LQR) [38], capable of controlling the machine over its entire operating envelope.

Transient design load cases (DLCs) [22, 23] are simulated using the aero-servo-elastic model and its controller. The results are post-processed to determine the maximum tip deflection and to extract at a number of span-wise verification sections the envelope loads, i.e. the maximum and minimum values of the internal stress resultants. At each verification section, maximum stresses and strains are computed at a number of verification spots on the cross section from the envelope loads, using recovery relations [34] obtained by the sectional analysis with ANBA. At the same verification spots, fatigue damage is computed from the stress time histories through rain-flow counting and the associated Markov matrices. The computed maximum tip deflection and the maximum stresses, strains and fatigue at each verification spot for each verification section are enforced as inequality constraints for the optimization problem, including the necessary safety factors.

A Campbell diagram of the machine is computed using the aero-elastic model. A design free of resonant conditions is obtained by constraining the placement of natural frequencies away from strong harmonic excitations; here this was obtained by simply prescribing a given minimum gap between the first blade flap frequency and the three-per-rev at the rated rotor speed, enforced as an inequality constraint in the optimization.

Additional inequality constraints are defined to enforce conditions on the design variables, such as a maximum thickness rate of change to account for typical values of ply tapering.

From the structural configuration of the blade and its sectional description, the total mass can be readily computed, accounting also for the non-structural mass due to surface coating, foam core, resin take-up, junction adhesive, etc. The total mass defines the cost function for the optimization problem; mass is used here because it is a good overall indicator of cost, and a reliable cost model was not available.

The optimization is run until convergence, using a Sequential Quadratic Programming (SQP) algorithm [39] with gradients computed by finite differences. For each new instantiation of the design variables, the 2D cross-sectional analysis is repeated, generating a new blade model and hence a new aero-servo-elastic wind turbine model. For each new model, the associated controller is re-tuned [20], and the necessary analyses repeated to update cost function and constraints. To reduce the computational cost and minimize the number of evaluations of the full set of DLCs, which is the most expensive part of the optimization, an outer iteration is used where the loads are temporarily frozen until the blade mass has converged and all constraints are satisfied; loads are then updated at the next iteration by repeating the DLCs, as explained in detail in Ref. [20].

At convergence of the blade optimization conducted at the coarse level using 2D cross-sectional

and aero-servo-elastic beam-based models, a 3D CAD solid model of the blade is generated automatically by lofting the computed blade geometry. The CAD model accounts for all blade parts including webs, web core, spar caps, leading and trailing edge reinforcements, internal skin, skin core and external skin, associated with the corresponding material properties and laminate characteristics. Meshing of the solid model with **HyperMesh** [40] automatically generates a 3D FEM model of the blade, using either shell or solid elements, the former option having been used in the present work.

The 3D FEM model of the blade is used for refining the design performed using the quasi-3D cross-sectional and beam models, as explained in the following.

At first, the blade mass is computed from the detailed 3D FEM model, this way improving the estimate of the problem cost function.

Next, static deflection analyses are conducted on the complete 3D model under all loading conditions that contribute to the definition of the load envelope. Such analyses are aimed at verifying the satisfaction of the stress and strain constraints, since the 3D model can capture effects that sectional and beam models cannot describe accurately, for example at the beginning and ending sections of the shear webs or in regions of rapid span-wise variations of the geometry. For each analysis, the aerodynamic chord-wise pressures are reconstructed using equivalent triangular distributions which are applied to the blade external nodes, while the inertial loads are applied to the sectional centroids.

A detailed fatigue analysis is performed based on loads obtained during the turbulent aero-servo-elastic simulations. Satisfaction of the fatigue constraints is verified at those spots where the coarse-level damage index is higher than a user-defined value, resulting in a considerable computational time saving (see Ref. [21] for details).

If some design inequality constraints are not satisfied, a heuristic approach is used where the constraint bounds are modified proportionally to the amount of the constraint violation, thereby making the bounds stricter. This way, the modified constraints will make their effects felt at the next iteration at the coarse quasi-3D level. For example, say that, at the end of the  $i$ th coarse level optimization, the maximum stress at a verification spot  $\sigma_{\max, \text{coarse}}^{(i)}$  satisfied the desired condition  $\sigma_{\max, \text{coarse}}^{(i)} \leq \sigma_{\text{adm}}$ , where  $\sigma_{\text{adm}}$  is the admissible stress. Suppose now that, at the fine level, the stress at that same point is  $\sigma_{\max, \text{fine}}^{(i)} > \sigma_{\text{adm}}$ , i.e. the allowable stress constraint is violated. To correct for this, at the  $(i + 1)$ th coarse iteration we set  $\sigma_{\text{adm}} = \sigma_{\text{adm}} \sigma_{\max, \text{coarse}}^{(i)} / \sigma_{\max, \text{fine}}^{(i)}$ , which is equivalent to making the local bound stricter. This modification of the constraint bound accounts for the fact that, for a given blade topology, the ratio between stresses computed at the coarse and fine levels remains roughly constant in the case of moderate variations of thicknesses of the structural elements between two consecutive macro iterations. In other words, since it is not possible to directly improve the model at the coarse level stage, given that the coarse representation is blind to the causes of discrepancy between stresses, the solution used here is to modify the constraint bound, in this way making the coarse level analysis feel the loop-closure effects of the fine level solution.

Finally, a non-linear buckling analysis is performed under the maximum tip deflection loads. Here again, if buckling is detected, the skin core thickness is increased using a heuristic approach. The modified core thickness modifies the non-structural mass of the cross-sectional model, this way again closing the loop between fine and coarse level analyses.

Based on the updated constraint conditions and updated model computed at the 3D FEM analysis level, new 2D sectional models are generated which in turn define a new beam model, and the complete process is repeated. Typically, very few iterations between the coarse and fine levels are necessary for convergence.

### 3 Design of Coupled Blades for Passive Load Mitigation

#### 3.1 Fully Coupled Blades

At first, we consider the case of fully coupled designs, where fibers are rotated in the skin and/or the spar caps for the whole span-wise extension of the blade.

The baseline uncoupled design used for comparison is that of a 45 meter rotor blade for a Class-III A 2MW HAWT. The blade structural layout uses a box-type three cell configuration, with a single cap confined within the two shear webs. The shear webs are parallel and planar, i.e. they do not follow the twist of the airfoils, as illustrated in Figure 2. Some of the main blade parameters and material types used are reported in Table 1.

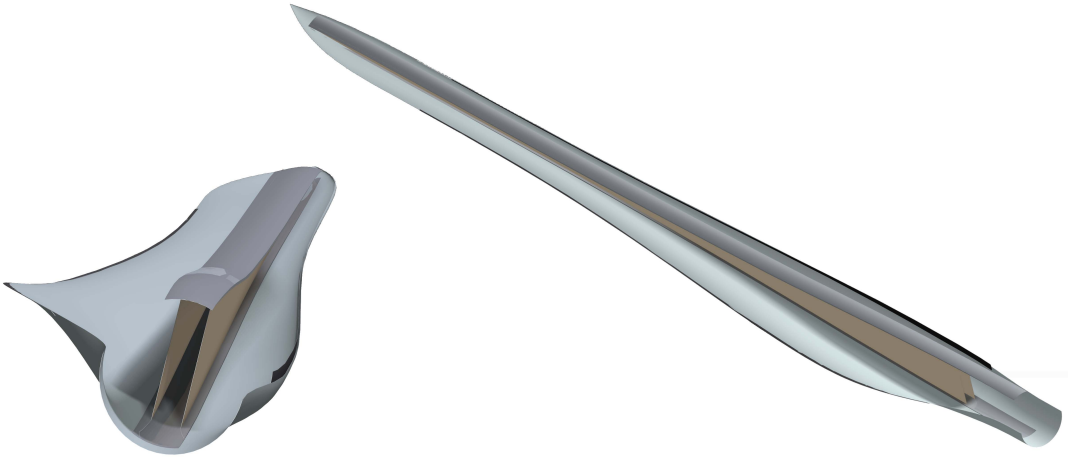


Fig. 2: Blade structural layout.

Tab. 1: Blade structural configuration parameters and material types.

	Starting section (% span)	Ending section (% span)	Material type
Skin	0	100	Stitched triaxial -45/0/+45 fiberglass
Spar caps	3	97.8	Unidirectional fiberglass
Shear webs	10	97.8	Stitched biaxial -45/+45 fiberglass
Trailing and leading edge reinforcements	10	80	Unidirectional fiberglass

To better highlight the characteristics of the solution space, at first the six distinct blade design configurations of Table 2 are considered.

The blades are designed using DLC 1.2, 1.4, 1.5, 1.6, 1.7, 2.2, 2.3 and 6.1 [22], with a maximum tip deflection of 5 meters, and first flap frequency placement and max stress/strain and fatigue constraints. The resulting six optimal designs, each satisfying exactly the same constraints, are then compared in terms of various performance metrics, including load envelope, hub and tower base DELs, and pitch ADC. The latter quantity is defined here as

$$\text{ADC} = \frac{1}{T} \sum_k F_{V_k} \int_0^T \frac{\dot{\beta}(t, V_k)}{\dot{\beta}_{\max}} dt, \quad (1)$$

Tab. 2: Blade models and their fiber rotations (Sk: fiber rotation in the skin; SC: fiber rotation in the spar caps).

Model name	Skin [deg]	Spar caps [deg]
Sk+10	10	0
Sk+20	20	0
Sk+30	30	0
SC+05	0	5
SC+10	0	10
Sk+20&SC+05	20	5

where  $\dot{\beta}$  is the blade pitch rate and  $\dot{\beta}_{\max}$  its maximum allowable value,  $V_k$  the mean wind speed of the  $k$ th turbulent DLC 1.2 of duration  $T$ , and  $F_{V_k}$  the occurrence of  $V_k$  in the machine lifetime according to the given Weibull distribution. Blade DELs are not included in the comparison, since each blade satisfies the fatigue constraints corresponding to a 20 year lifetime.

Table 3 reports, for each optimal blade design, the status (active or non-active) of each design constraint. For all models the frequency placement and the max tip deflection constraints are active at convergence, and therefore the design of the blade is driven by its flap bending stiffness. Furthermore, it appears that the fatigue damage constraint is active in the regions of the blade with the largest chord values. This highlights the need to include fatigue constraints in the optimization procedure, for the complete in-plane stress tensor. In fact, the rotation of the fibers has, on the one hand, the positive effect of reducing loads but, on the other, involves a load transfer from the stronger component of the laminate, the fiber, to its weakest one, the matrix, and this effect grows when increasing the angle of fiber rotation. Clearly, if the fatigue assessment was performed only on the stresses computed along the fiber directions, it would not be possible to capture the effects of fatigue on the matrix.

Tab. 3: Constraint status for the six optimal designs (A: active; N: non-active).

Model/Constraint	Stress/strain	Flap freq.	Max tip defl.	Fatigue
Sk+10	N	A	A	A: skin from 10% to 40% span
Sk+20	N	A	A	A: skin from 10% to 40% span
Sk+30	N	A	A	A: skin from 10% to 40% span
SC+05	N	A	A	A: skin at 40% span
SC+10	N	A	A	A: skin from 10% to 40% span A: spar caps at 10% span
Sk+20&SC+05	N	A	A	A: skin from 10% to 40% span

Figure 3 plots along the non-dimensional span-wise coordinate  $\eta \in [0, 1]$  the coupling coefficient  $\alpha = K_{bt}/\sqrt{K_b K_t}$ , as defined in Ref. [7], where  $K_b$  is the local flap-wise bending stiffness,  $K_t$  the torsional one, and  $K_{bt}$  the coupled bend-twist stiffness term. Although the present designs only make use of fiber glass material (cf. Table 1), the values of the figure are in line with those of Ref. [19], which made use of carbon fiber in the spar caps. Moreover, it is interesting to notice that coupling does not necessarily always increase with fiber angle, since the thicknesses of the structural elements change so as to satisfy the design constraints. For example, by increasing the angle of 10 deg from model Sk+20 to the design solution Sk+30, the figure shows that the span-wise coupling is largely unaffected.

Figure 4 reports the percent mass increase of the six optimal designs with respect to the uncoupled baseline model. It appears that mass increases rapidly with increasing fiber rotation angle. For example, this effect is evident by looking at the trend for the three solutions with fiber

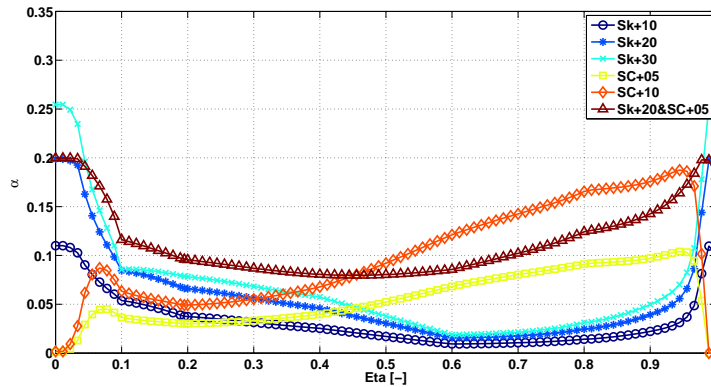


Fig. 3: Coupling coefficient  $\alpha$  [7] for the six optimal designs.

rotations in the skin (Sk+10, Sk+20 and Sk+30), and the trend of the two solutions with fiber rotations in the spar caps (SC+05 and SC+10). It also appears that the mass rate of increase is much higher for spar cap fiber rotations than for skin ones. These effects are due to the fact that this blade is mainly driven by frequency placement and maximum tip deflection constraints, as shown in Table 3, so that, even if envelope loads and fatigue are reduced due to BTC, the blade structural components have to be thicker to restore the sectional stiffness and satisfy the design constraints. Therefore, since bending stiffness is largely dictated by the spar caps, the use of large fiber angles in the spar caps should be avoided to limit the impact on the blade mass.

The figure also shows that by distributing the coupling between skin and spar caps, as done in the sixth design configuration Sk+20&SC+05, one can obtain interesting sectional couplings (cf. Fig. 3) without incurring in large mass increases. In fact, using larger fiber rotations in the skin allows one to keep the angle in the spar caps close to small values, which in turn helps in limiting the reduction of sectional bending stiffness.

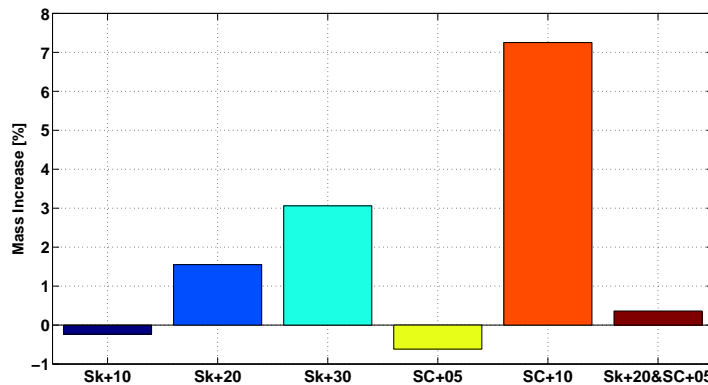


Fig. 4: Percent blade mass increase with respect to the uncoupled baseline model for the six optimal designs.

Figure 5 reports the values of mean power (at left) and blade pitch (at right) vs. mean wind speed, computed from turbulent simulations conducted according to DLC 1.2, for the six optimal designs and the reference baseline solution. The figure shows that all designs have essentially the same power production, as also confirmed by Table 4 that gives the annual energy production

(AEP) for the various blades. In fact, the necessary trim pitch settings in the partial and full power regions were adjusted so as to compensate the different deformations of the different blades. In particular, the figure shows on the right how pitch is lower in the partial region for coupled blades because twisting induced by bending tends to decrease the angle of attack, and this requires a lower pitch to achieve the same aerodynamic torque and rotor RPM at each given mean wind speed.

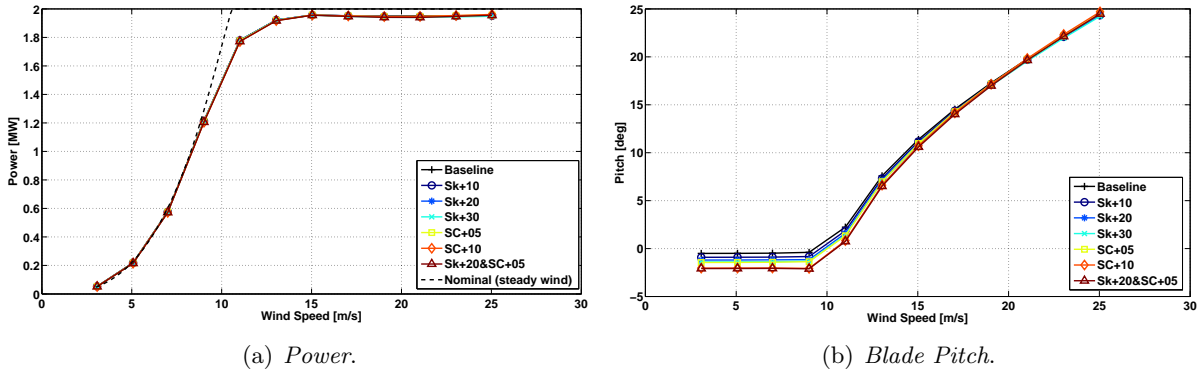


Fig. 5: Mean power in turbulent wind (left) and blade pitch setting (right) vs. mean wind speed for the six optimal design solutions and the reference baseline.

Tab. 4: Class A turbulent wind AEP as a percent fraction of the nominal steady wind  $AEP_{\text{nominal}}$ , for the six design solutions and the reference baseline model.

Model	$AEP/AEP_{\text{nominal}}$ (%)
Baseline	94.2%
Sk+10	94.2%
Sk+20	94.1%
Sk+30	94.0%
SC+05	94.0%
SC+10	93.7%
Sk+20&SC+05	93.7%

The effects of BTC on the envelope loads are illustrated in Fig. 6, which shows the percent reductions with respect to the baseline design for the hub (at left) and tower root (at right) loads. All configurations have very little effects on the hub forces, while the reductions on the hub moments are more noticeable. The effects on the hub moments are more pronounced with increasing coupling, except when the weight increase is excessive, as shown for example by the load reduction for SC+10 in the nodding moment, which is smaller than the one of SC+05. Similar observations can be made for the tower root moments.

The mechanism of load reduction of BTC blades is nicely illustrated by Fig. 6, which shows the angle of attack at a specific blade station during an extreme operative gust (EOG), a condition that defines the envelope tower base fore-aft moment. At the beginning of the gust, when loads are still small, the angles of attack of the various blades are very similar. Then, at the higher values of wind speed, the blades with higher coupling coefficients exhibit a lower angle of attack, because the increase in blade bending due to gust loads twists the blade section.

Figure 8 reports the DEL reductions at the hub and tower root with respect to the baseline configuration. All coupled models positively affect DELs, although even here one can notice some

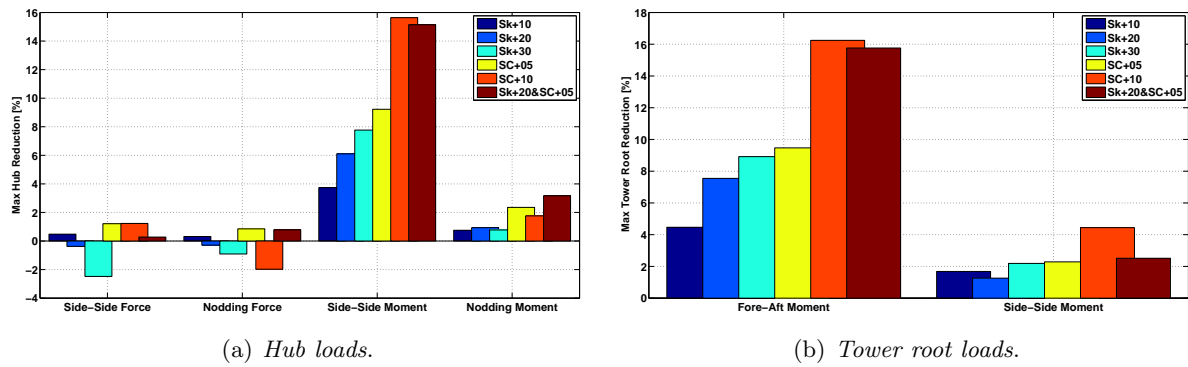


Fig. 6: Envelope load reductions at the hub (at left) and the tower root (at right) with respect to the baseline model for the six optimal designs.

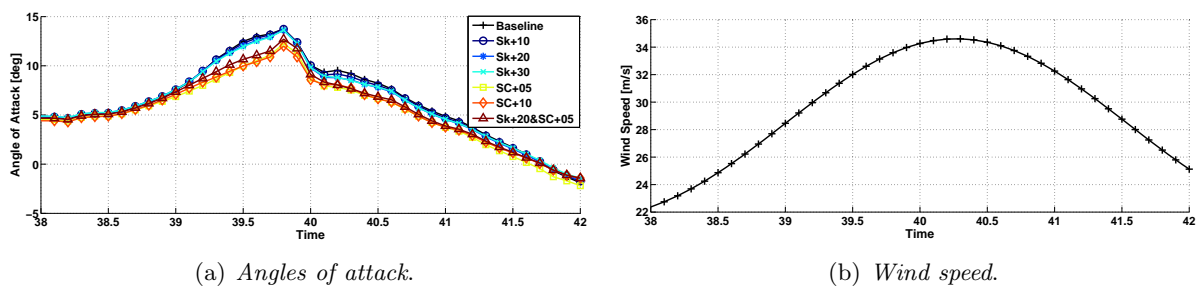


Fig. 7: Angle of attack time history (at left) at blade station  $\eta = 0.8$  for the wind gust (at right) corresponding to DLC 1.5 at 25 m/sec.

dependency on blade weight, for example by looking at the blade DEL reduction for SC+10 that is the same as the one of Sk+20&SC+05, which has somewhat smaller coupling but it is lighter.

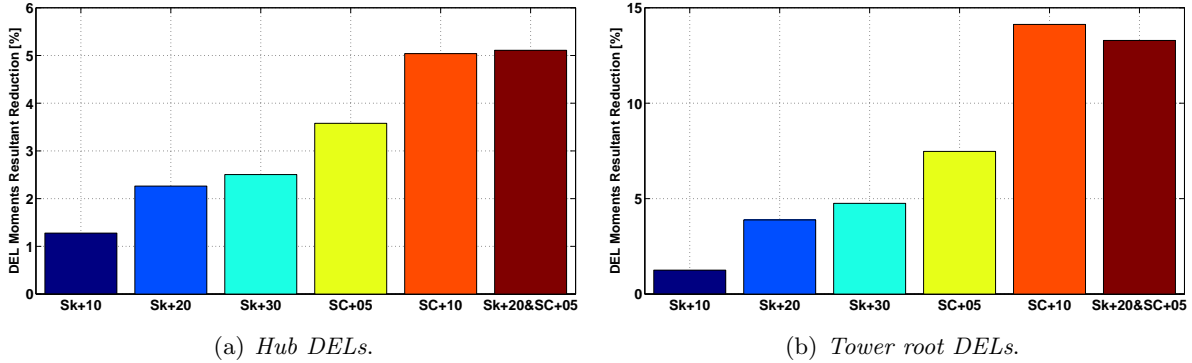


Fig. 8: DEL reductions at the hub (at left) and the tower root (at right) with respect to the baseline model for the six optimal designs.

A very interesting aspect of BTC blades is their positive effects on ADC. In fact, Fig. 9 shows that for all coupled models there is a large reduction in the duty cycle of the pitch actuator. This is due to the passive control effect of coupled blades: since these adaptive blades self-respond to turbulent fluctuations in the wind, the active control system pitches the blades less (since it feels less the effects of turbulence through its feedback loop), thereby reducing the effort on the pitch system.

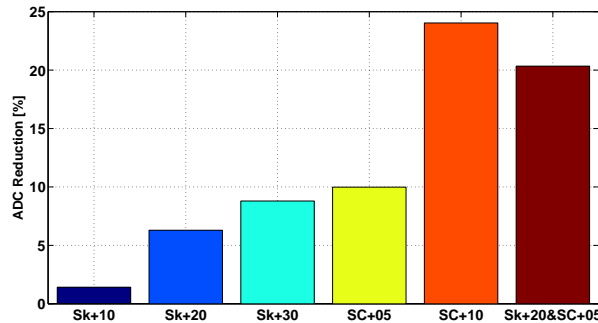


Fig. 9: ADC percent reduction with respect to the baseline model for the six optimal designs.

To better illustrate the effect on ADC of BTC blades, one can look at the pitch angle obtained in closed-loop operation in turbulent wind conditions. Figure 10 shows the pitch angle time history during DLC 1.2 at a mean wind speed of 11 m/sec. The figure highlights a markedly different behavior for the various models. For low wind speeds in the partial load region, i.e. around 360 sec at 11 m/sec, pitch angles are all constant and equal to their own respective trim values. When the wind speed starts to increase and oscillates between the partial and full load regions, pitch angles are modified by the feedback control loop, but in a different way for each model. The baseline model and the ones with lower degrees of coupling exhibit large pitch oscillations, while the more coupled models reach lower pitch values. For example, at time 390 sec the baseline model is subjected to an aggressive pitch control sequence, while SC+10 and Sk+20&SC+05 pass through the same wind event with a much smoother pitch input. These results clearly illustrate that the pitch controller, thanks to the self-reaction and built-in passive

control of BTC blades, has to react less aggressively to turbulent wind fluctuation, resulting in a lower effort on the pitch system and therefore in a reduced ADC.

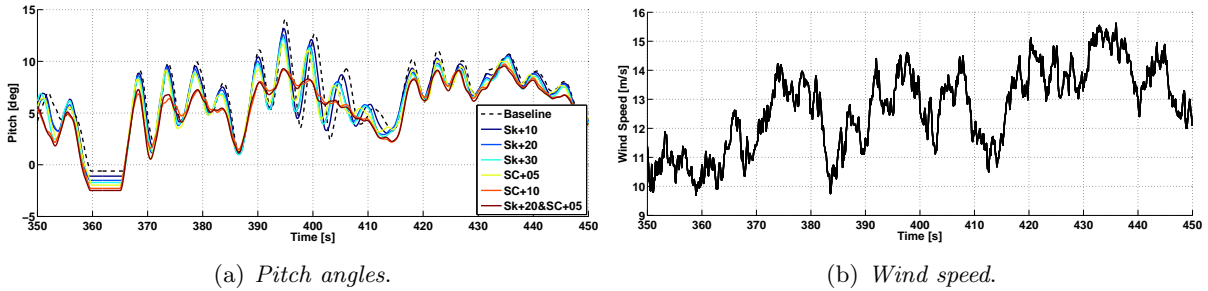


Fig. 10: Pitch angle time history (at left) for the turbulent wind (at right) corresponding to DLC 1.2.

These results indicate that Sk+20&SC+05 represents a good compromise solution, because it achieves interesting envelope, fatigue and ADC reductions with only a very modest weight increase. This is due to the fact that the blade has good levels of bend-twist coupling due to the synergistic use of fiber rotations in the spar caps and skin. In particular, the latter allows to limit the former to small values, which reduces the impact on spar cap thickness, in turn avoiding excessive penalties in terms of blade weight.

### 3.2 Partially Coupled Blades

In the first part of this study, it was shown that a BTC blade can achieve interesting improvements in all considered quality metrics, including maximum loads, fatigue damage and pitch actuation effort. The main limit of the solutions investigated so far is however the mass increases that invariably accompany these improvements. This is due to the fact that the design driving factors are the maximum tip displacement and the frequency placement constraints, which both depend directly on sectional stiffness.

It appears that a possible way to mitigate this effect is to rotate the fibers not throughout the whole blade span, as done previously, but only in its outboard sections. As a matter of fact, by limiting fiber rotations to selected span-wise sections, the blade is less affected by the associated stiffness drop, and this may result in a different mass configuration. Moreover, this can also help in satisfying fatigue constraints. In fact, the sections in proximity of the maximum blade chord are typically the ones that are more affected by fatigue damage. Avoiding fiber rotations in this part of the blade, and therefore allowing the material to better contribute to the bending stiffness, reduces the necessity to increase the thickness of the structural members so as to satisfy fatigue constraints.

To investigate this idea, we consider blade model Sk+20&SC+05, because it exhibits good quality metric improvements with only a modest mass increase. Five configurations are investigated, each one characterized by fiber rotations starting from a different span-wise location. The five different cases are shown in Fig. 11, and labeled F#, where # is the fiber rotation starting section in percent span. The first configuration, F0, is the fully coupled blade of the previous section. Each blade was obtained with the previously discussed constrained optimization procedure, and therefore each represents a constraint satisfying optimal design.

For each blade configuration, Table 5 reports the status (active or non-active) of each design constraint. The table highlights a first effect of the partially coupled design solutions. In fact, for

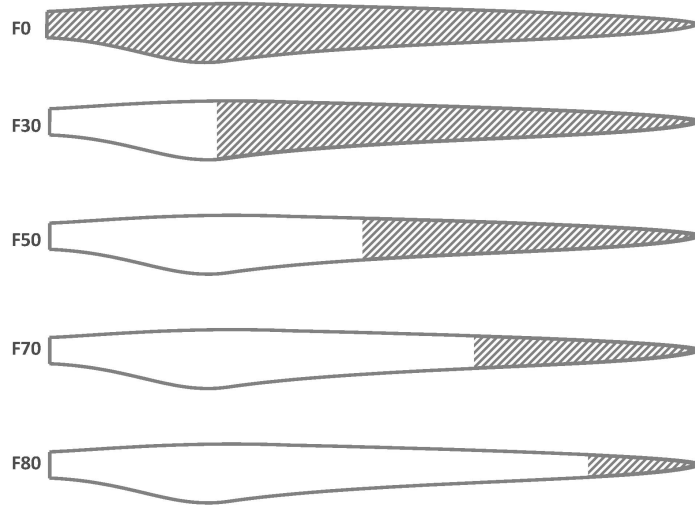


Fig. 11: Partially coupled blade models and their fiber rotation starting sections.

rotations between 30% and 70%, the fatigue constraint is no longer active. On the other hand, the constraint is active for the fully coupled blade F0 because fibers are rotated in the more critical area of maximum chord, while for F80 the coupling is too low and there is not enough load reduction to make the constraint inactive.

Tab. 5: Constraint status for the four partially coupled blades and the fully coupled one F0 (A: active; N: non-active).

Model/Constraint	Stress/strain	Flap freq.	Max tip defl.	Fatigue
F0	N	A	A	A: skin from 10% to 40% span
F30	N	A	A	N
F50	N	A	A	N
F70	N	A	A	N
F80	N	A	A	A: skin from 10% to 30% span

Figure 12 reports the percent blade mass increase for the four partially coupled blades and the fully coupled one, with respect to the baseline uncoupled solution. From the figure, it clearly appears that partial coupling has a beneficial effect on blade weight. Specifically, the minimum blade weight is achieved for F70, which exhibits a mass decrease of about 2.8% with respect to the uncoupled baseline and a decrease of about 3.2% with respect to the fully coupled solution F0.

Figure 13 shows the percent reductions with respect to the baseline for the hub (at left) and tower root (at right) loads. In general, the load reduction diminishes with the fiber rotation starting section moving outward. This is because the resulting blades are less coupled, and therefore there is less passive load reduction. Also, it should be noticed that F30 is either only slightly worse than F0, because of reduced coupling, or slightly better in some cases, because of its reduced weight.

Figure 14 shows that the effects of partial coupling on DELs present a very similar trend to the case of the envelope loads. In fact, here again only F30 exhibits reductions which are similar to the fully coupled case of F0, while F50 to F80 pay for a diminished coupling effect that is less

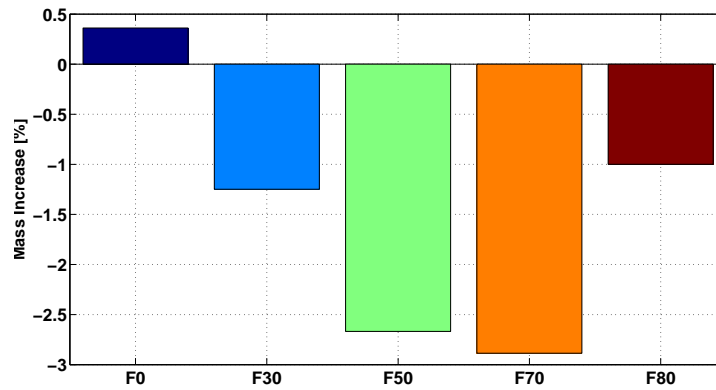


Fig. 12: Percent blade mass increase with respect to the uncoupled baseline model for the four partially coupled designs and the fully coupled one F0.

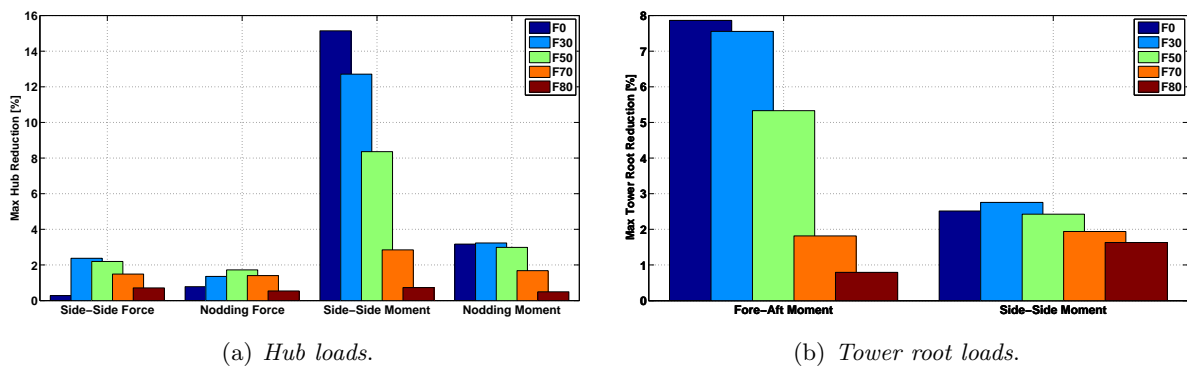


Fig. 13: Envelope load reductions at the hub (at left) and the tower root (at right) with respect to the baseline model for the four partially coupled designs and the fully coupled one F0.

capable of reducing loads. The figure presents the case of the hub loads, but very similar results are obtained also for the tower loads.

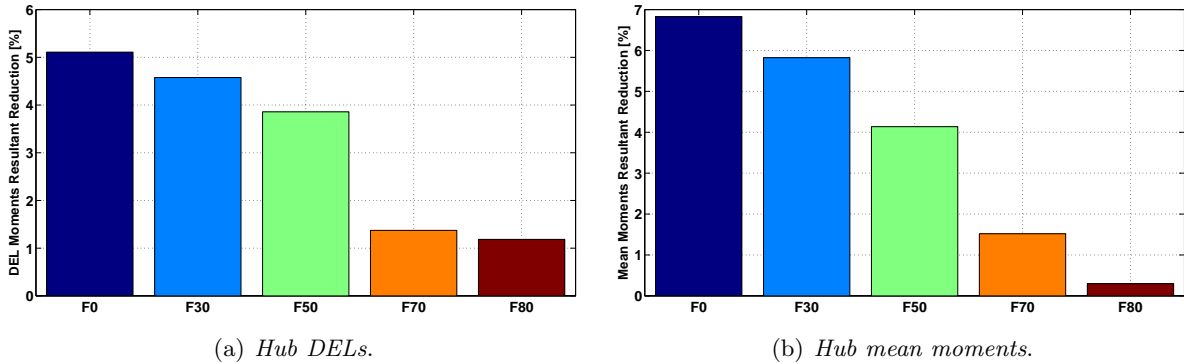


Fig. 14: Hub DEL (at left) and mean (at right) moment resultant reduction with respect to the baseline model for the four partially coupled blades and the fully coupled one F0.

Finally, Fig. 15 shows the effects of partial coupling on ADC. Here again, fiber rotation sections close to the root only suffer a modest loss of performance with respect to the fully coupled blade, while the more outboard sections significantly affect coupling, and hence incur in significant performance penalties. For example, for the F50 model the reduction is 50% lower than the one of the fully coupled blade.

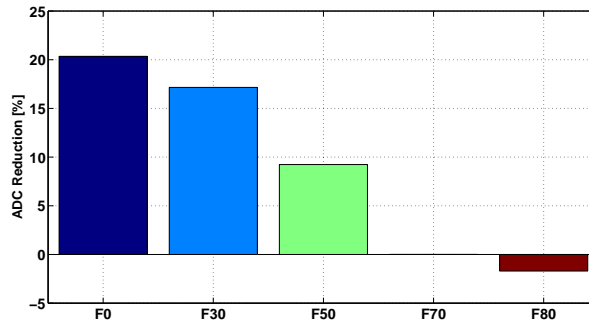


Fig. 15: ADC percent reduction with respect to the baseline model for the four partially coupled designs and the fully coupled one F0.

From this analysis it appears that a partially coupled blade can achieve improvements in all performance metrics, while at the same time weighing less than an uncoupled blade. In fact, rotating the fibers only in the outboard sections of the blade, and not close to its root, affects less the frequency placement and the maximum tip deflection constraints, so that the thickness of the structural components does not need to be increased (actually, it can be somewhat reduced). An interesting tradeoff appears to be represented by the F30 model, because it reduces the blade mass of almost 1.5% with respect to the fully coupled blade, while achieving about the same amount of load reduction.

## 4 Integration of Passive and Active Load Control

Active load control systems exploit a power source to move the whole blade, or a part of it, so as to reduce loads due to turbulence, gusts and asymmetry in the inflow. Generally these systems require sensors to measure the wind turbine response and drive, through a feedback loop, a suitable motion strategy. Recently, several IPC formulations have been proposed, demonstrating a significant potential for fatigue load reduction [25, 26, 27, 28, 29, 30, 31, 32, 33, 24]. In fact, changing the pitch of each blade independently allows for the reduction of the lowest load harmonics, including their mean value. However, one of the possible drawbacks of active load control is its effect on the actuators and their design: constantly pitching the blade increases the actuator duty cycle, and hence its wear. This, in turn, requires more expensive and larger actuators, inducing a tradeoff with the advantages brought by IPC.

Since BTC blades were shown in the previous section to allow for a reduction in ADC, it seems interesting to try to combine the two load control technologies. In fact, on the one hand, since both BTC and IPC can reduce loads, by combining them one may obtain a synergistic effect. On the other hand, since BTC tends to reduce ADC and IPC to increase it, by combining the two one can hope to obtain significant load reductions with reduced ADC increases. This idea is explored next.

For the present investigation, we consider the partially coupled blade configuration F30, because it achieves a good tradeoff between load and weight reduction.

The individual pitch controller is based on the architecture proposed in Ref. [26], and depicted in Fig. 16. The controller is driven by blade root moments, which are Coleman transformed in a nacelle-fixed frame of reference to yield the rotor tilt and yaw moments. Two independent proportional integral derivative (PID) controllers compute two fixed frame control inputs by trying to drive the tilt and yaw moments to zero. In turn, the fixed frame inputs are back-transformed into the rotating frame using the inverse Coleman transformation, an operation that generates the individual pitch control inputs. Such inputs are superimposed to the ones computed by a collective pitch and torque controller implemented with the speed-scheduled LQR formulation of Ref. [38], whose roles are the regulation of the machine around a given set point and the reaction to gusts.

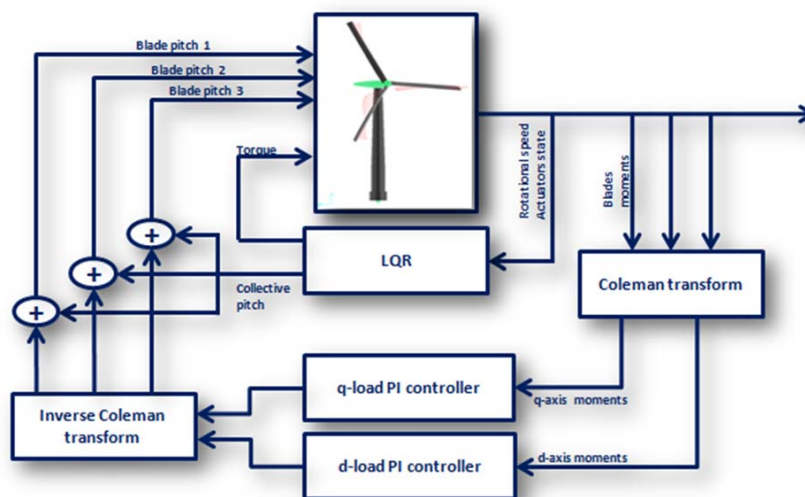


Fig. 16: Individual blade pitch control architecture.

By adjusting the gains of the IPC PID controllers, one can tune within a certain range the level of individual blade pitch activity, consequently affecting the level of load reduction and of ADC increase. For this study, two different sets of gains were selected: the first has lower gains and therefore only a moderate ADC increase, while the second one has higher gains and a more aggressive behavior.

In the following, six combinations of blade and controller designs are considered. The baseline is taken to be the uncoupled blade with the LQR collective pitch controller. In addition, we consider the partially coupled blade F30 with the collective trimmer, termed BTC in the following figures. The uncoupled blade used with the first set of gains is labeled IPC1, and IPC2 when the more aggressive set of gains is used. Similarly, the partially coupled blade is termed BTC+IPC1 when used with the first set of gains, and BTC+IPC2 with the second. All configurations achieve essentially the same power production, with differences in their respective AEPs below 1%.

Figure 17 shows, for the six different combinations, ADC percent variations with respect to the baseline as a function of mean wind speed  $V$ , as obtained through turbulent DLC 1.2 simulations.

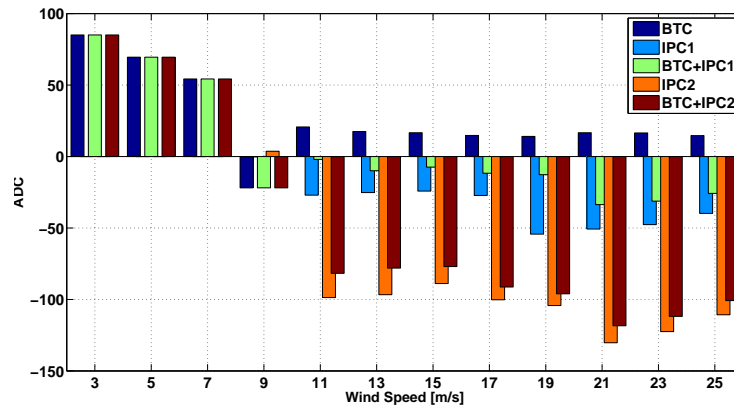


Fig. 17: ADC reductions with respect to the baseline model vs. mean wind speed.

In region II, below rated, the use of BTC improves ADC; however, ADC is very small in this region which is mostly characterized by a torque control strategy, and hence these effects are negligible. The full power region III is more interesting. Here it appears that, as expected, BTC improves ADC while IPC, whether aggressively tuned or not, invariably implies a worsening of the ADC parameter. Furthermore, the less aggressive tuning of IPC1 generates ADC increases in excess of 50%, while the more aggressive tuning of IPC2 brings the ADC increase to over 130%.

It is interesting to look at the combined models BTC+IPC1 and BTC+IPC2, which show a synergistic combination of the effects of the active and passive load reducing systems. Indeed for these models ADC increases are smaller than in the case when the uncoupled blade is used with IPC. Up to a wind speed of 19 m/sec, BTC+IPC1 has a maximum ADC increase of about 10%, which should be compared to the almost 30% of IPC1. For model BTC+IPC2, variations are smaller but still relevant. Weighting with the Weibull distribution, the lifetime ADC for the BTC model shows a reduction of almost 20%, while for IPC1 it increases of around 25% and for BTC+IPC1 it has only a slight increase around 5%. This last result shows that the combination of the passive and active control strategies leads to an actuator duty cycle that is essentially equal to the one of the baseline blade with purely collective blade pitch control.

Figure 18 shows, for the six combinations, the hub DELs and mean moments vs. mean wind speed. It appears that, here again, the active and passive technologies have synergistic effects. In

fact, models BTC+IPC1 and BTC+IPC2 have a higher load reduction than models BTC, IPC1 and IPC2, i.e. when using only either a passive or an active solution. Furthermore, it should be stressed once again that the load reductions achieved by BTC+IPC1 are obtained with roughly the same ADC as the baseline case.

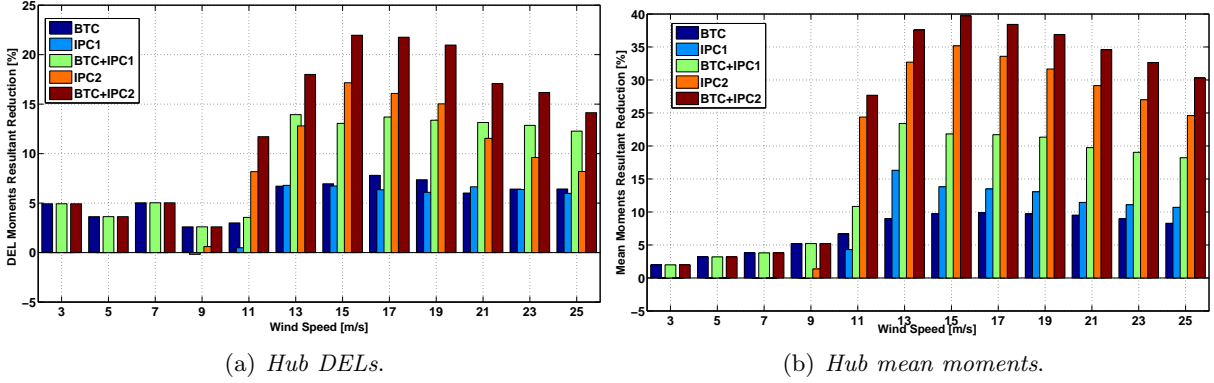


Fig. 18: Hub DELs (at left) and mean moments (at right) reductions with respect to the baseline model vs. mean wind speed.

## 5 Conclusions

In this paper we have studied the design of BTC blades, and we have considered the possible synergies between passive and active load mitigation. The blade design was conducted within a novel comprehensive multi-level constrained optimization approach. The design process alternates between a multibody beam model augmented with 2D FEM cross sectional sub-models and a fine scale 3D FEM detailed model of the blade. The former enables the numerous transient aero-servo-elastic analyses required to compute loads and deflections throughout the lifetime of the machine, while the latter makes it possible to conduct detailed local verifications of the design; loop closure between the two levels is accomplished by a heuristic approach that modifies when necessary some coarse level design constraints.

Based on the study conducted herein, it is possible to draw the following conclusions:

- The use of a constrained optimization-based approach to design is crucial because it allows one to compare alternative solutions that satisfy the same design requirements, and that hence are all viable.
- The synergistic use of fiber rotations in the skin and spar caps is beneficial in terms of blade weight. In fact, fiber rotations in the skin allow one to limit rotations in the spar caps, which otherwise would need to be thickened so as to contrast bending stiffness loss. This way, good levels of bend-twist couplings were obtained here without the need to resort to more performing materials, such as carbon fiber, while keeping blade weight largely unaffected.
- Avoiding fiber rotations from the blade root to about the span of maximum chord is also beneficial in terms of blade weight. In fact the additional couplings generated in this region by fiber rotations are not only modest, but are also more than offset by increased fatigue damage and reduced bending stiffness, which both lead to weight increases. This solution also suggests the use of different fiber angles in different span-wise segments of the blade,

aimed at the optimization of the span-wise distribution of couplings, which however was not investigated here.

- By combining skin and spar cap fiber rotations with partial span-wise coupling, it appears possible to design blades that exhibit significant load reduction capabilities, and yet are somewhat lighter than standard uncoupled blades.
- BTC blades not only reduce maximum and fatigue loads, but also imply a reduced pitch ADC. In fact, the blade self-reacts to wind fluctuations, this way taking some of the burden off the controller. Since IPC tends to increase ADC, which is one of the main reasons why IPC has not yet been widely adopted by manufacturers, one might argue that BTC blades might also be used to make IPC more economically viable in future designs.
- Although a more comprehensive study on various wind turbines of different sizes would be necessary to draw final conclusions, it appears that the amount of load reduction enabled by BTC blades is of the same order of magnitude of that allowed by IPC.
- The combination of passive, via BTC, and active, via IPC, technologies leads to load reductions that are higher than it would be possible by the use of each single one of the two approaches. In the end, the limit of achievable load reduction is also probably due to the physics of the mitigation mechanism itself, that in both cases is due to a change of angle of attack. This is constant throughout the blade span for IPC, since the whole blade is pitched, while it is slowly varying along the span for BTC, but in both cases there is not a way to locally modify the flow conditions in response to small scale spatial and temporal wind fluctuations. Therefore, in both cases, the attenuation is limited to the larger spatial and slower turbulent scales, and an increase in bandwidth could only be achieved with a distributed, more localized and faster response, as for example with flaps, tabs or other devices.

Although an effort was made throughout this work to propose solutions that would not radically alter the way current blades are designed and manufactured, since this would raise more questions than one could answer, it is clear that the actual benefits of the proposed solutions need more careful scrutiny and further investigations, so as to account also for a number of manufacturing and technological considerations that were not addressed here. In the end, the performance index of a wind turbine design is the cost of energy, so that all implications of the adoption of a specific technology need to be factored in so as to fully understand all trade-offs.

## References

- [1] Veers PS, Bir G, Lobitz DW. Aeroelastic tailoring in wind-turbine blade application. Wind-power '98, AWEA Annual Conference and Exhibition, Bakersfield, CA, April 27 – May 1, 1998.
- [2] Lobitz DW, Veers PS, Eisler GR, Laino DJ, Migliore PG, Bir G. *The Use of Twist-Coupled Blades to Enhance the Performance of Horizontal Axis Wind Turbines*. Sandia Report SAND 2001-1303, Sandia National Laboratories, Albuquerque, NM, May 2001.
- [3] Liebst BS. Wind turbine gust load alleviation utilizing curved blades. *Journal of Propulsion* 1986; **2**:371–377.

- 
- [4] Zuteck M. *Adaptive Blade Concept Assessment: Curved Planform Induced Twist Investigation*. Sandia Report SAND 2002-2996, Sandia National Laboratories, Albuquerque, NM, October 2002.
- [5] Lobitz DW, Veers PS, Migliore PG. Enhanced performances of HAWTs using adaptive blades. Wind Energy '96, ASME Wind Energy Symposium, Houston, January 29 – February 2, 1996.
- [6] Lobitz DW, Laino DJ. Load mitigation with twist-coupled HAWAT blades. '99 ASME Wind Energy Symposium, Reno, January 11–14, 1999.
- [7] Lobitz D, Veers PS, Laino D. Performance of twist-coupled blades on variable speed rotors. AIAA 2000-0062, 2000 ASME Wind Energy Symposium, Reno, January 10–13, 2000.
- [8] Ong C, Tsai S. *Design, Manufacture and Testing of a Bend-Twist D-spar*. Sandia Report SAND 99-1324, Sandia National Laboratories, Albuquerque, NM, 1999.
- [9] Griffin DA. *Evaluation of Design Concepts for Adaptive Wind Turbine Blades*. Sandia Report SAND 2002-2424, Sandia National Laboratories, Albuquerque, NM, August 2002.
- [10] de Goeij W, van Tooren M, Beukers A. Implementation of bending-torsion coupling in the design of a wind-turbine rotor-blade. *Applied Energy* 1999; **63**:91–207.
- [11] Zayas JR, Jones PL, Holman A. *CX-100 and TX-100 Blade Field Tests*. Sandia Report SAND 2005-7454, Sandia National Laboratories, Albuquerque, NM, December 2005.
- [12] Berry D. *Design of 9-Meters Carbon-Fiberglass Prototype Blades: CX-100 and TX-100*. Sandia Report SAND 2007-0201, Sandia National Laboratories, Albuquerque, NM, September 2007.
- [13] Berry D. *TX-100 Manufacturing Final Project Report*. Sandia Report SAND 2007-6066, Sandia National Laboratories, Albuquerque, NM, November 2007.
- [14] Ashwill TD. Passive load control for large wind turbines. 51st AIAA/ASME/ASCE/AHS/ASC Structures, Structural Dynamics, and Materials Conference, Orlando, Florida, April 12–15, 2010.
- [15] Resor B, Paquette J, Laird D, Griffith DT. An evaluation of wind turbine blade cross section analysis techniques. 51st AIAA/ASME/ASCE/AHS/ASC Structures, Structural Dynamics, and Materials Conference, Orlando, Florida, April 12–15, 2010.
- [16] Locke J, Valencia U. *Design Studies for Twist-coupled Wind Turbine Blades*. Sandia Report SAND 2004-0522, Sandia National Laboratories, Albuquerque, NM, USA, 2004.
- [17] Wetzel KK, Locke JE. Uncoupled and twist-bend coupled carbon-glass blades for the LIST turbine. AIAA 2004-170, 42nd AIAA Aerospace Sciences Meeting and Exhibit, Reno, January 5–8, 2004.
- [18] Lin H-J, Lai W-M. A study of elastic coupling to the wind turbine blade by combined analytical and finite element beam model. *Journal of Composite Materials* 2010; **44**:2643–2665.
- [19] Capellaro M, Kühn M. Boundaries of bend twist coupling. The Science of Making Torque from Wind, Crete, Greece, June 28–30, 2010.

- 
- [20] Bottasso CL, Campagnolo F, Croce A. Multi-disciplinary constraint optimization of wind turbines. *Multibody System Dynamics* 2011; DOI 10.1007/s11044-011-9271-x.
- [21] Bottasso CL, Campagnolo F, Croce A, Dilli S, Nielsen MB, Tibaldi C. Optimization of wind turbine rotor blades by integrated sectional/multibody/3DFEM analysis. 2011; in preparation for submission.
- [22] Anonymous. *Wind Turbines - Part 1: Design Requirements*. International Standard IEC 61400-1, 2005.
- [23] Anonymous. *Guideline for the Certification of Wind Turbines*. Germanischer Lloyd, Hamburg, 2010.
- [24] Bottasso CL, Croce A, Devecchi D, Riboldi CED, Nam Y. Multi-layer control architecture for the reduction of deterministic and non-deterministic loads on wind turbines. *Wind Energy* 2011; accepted, to appear.
- [25] Bossanyi E. The design of closed loop controllers for wind turbines. *Wind Energy* 2000; **3**:149–163.
- [26] Bossanyi E. Individual blade pitch control for load reduction. *Wind Energy* 2003; **6**:119–128.
- [27] Bossanyi E. Wind turbine control for load reduction. *Wind Energy* 2003; **6**:229–244.
- [28] Bossanyi E. Developments in individual blade pitch control. The Science of Making Torque from Wind, Delft, The Netherlands, April 19–21, 2004.
- [29] Bossanyi E. Further load reductions with individual pitch control. *Wind Energy* 2005; **8**:481–485.
- [30] van Engelen T. Design model and load reduction assessment for multi-rotational model individual pitch control. European Wind Energy Conference (EWEC 2006), Athens, Greece, February 27 – March 1, 2006.
- [31] Geyler M, Caselitz P. Individual blade pitch control design for load reduction on large wind turbines. European Wind Energy Conference (EWEC 2007), Milano, Italy, May 7–10, 2007.
- [32] Kanev S, van Engelen T. Exploring the limits in individual pitch control. European Wind Energy Conference (EWEC 2009), Marseille, France, March 16–19, 2009.
- [33] Leithead W, Neilson V, Dominguez S. Alleviation of unbalanced rotor loads by single blade controllers. European Wind Energy Conference (EWEC 2009), Marseille, France, March 16–19, 2009.
- [34] Giavotto V, Borri M, Mantegazza P, Ghiringhelli GL. Anisotropic beam theory and applications. *Computers & Structures* 1983; **16**:403–413.
- [35] Bauchau OA. *Flexible Multibody Dynamics*. Springer, Solid Mechanics and its Applications, Vol. 176, 2011.
- [36] Bauchau OA, Bottasso CL, Trainelli L. Robust integration schemes for flexible multibody systems. *Computer Methods in Applied Mechanics and Engineering* 2003; **192**:395–420.

- 
- [37] Bottasso CL, Croce A. *Cp-Lambda: User's Manual*. Dipartimento di Ingegneria Aerospaziale, Politecnico di Milano, 2006–2011.
- [38] Bottasso CL, Croce A, Riboldi CED., Nam Y. Power curve tracking in the presence of a tip speed constraint. *Renewable Energy* 2011; accepted, to appear.
- [39] Matlab, The MathWorks Inc., 3 Apple Hill Drive, Natick, MA 01760-2098, USA, [www.mathworks.com](http://www.mathworks.com).
- [40] HyperMesh, Altair Engineering, 1820 Big Beaver Rd, Troy, MI 48083, USA, [www.altair.com](http://www.altair.com).